Electrochemistry

International Edition: DOI: 10.1002/anie.201511673
German Edition: DOI: 10.1002/ange.201511673

A Strategy for Configuration of an Integrated Flexible Sulfur Cathode for High-Performance Lithium–Sulfur Batteries

*Hongqiang Wang, Wenchao Zhang, Huakun Liu, and Zaiping Guo**

Abstract: *Lithium–sulfur batteries are regarded as promising candidates for energy storage devices owing to their high theoretical energy density. The practical application is hindered, however, by low sulfur utilization and unsatisfactory capacity retention. Herein, we present a strategy for configuration of the sulfur cathode, which is composed of an integrated carbon/sulfur/carbon sandwich structure on polypropylene separator that is produced using the simple doctor-blade technique. The integrated electrode exhibits excellent flexibility and high mechanical strength. The upper and bottom carbon layers of the sandwich-structured electrode not only work as double current collectors, which effectively improve the conductivity of the electrode, but also serve as good barriers to suppress the diffusion of the polysulfide and buffer the volume expansion of the active materials, leading to suppression of the shuttle effect and low self-discharge behavior.*

Lithium–sulfur (Li-S) batteries show great potential for the next generation of lithium-ion batteries, as sulfur features high theoretical capacity (1675 mAh g^{-1}), high specific energy density (2600 Wh kg^{-1}), cost effectiveness, and nontoxicity.[1–3] Nevertheless, the broad application of Li-S batteries is limited by several persistent problems, including the low electronic conductivity of sulfur and its discharge product, the high solubility and diffusivity of polysulfide intermediates, and the related side reaction shuttle effect, as well as volume expansion caused by the intercalation of Li into the sulfur.[4–7] Therefore, the key points for the development of Li-S batteries are to improve the conductivity of the sulfur cathode, enhance the tolerance for volume expansion, and maintain the soluble polysulfides within the cathode region. In the past few years, much effort has been devoted to addressing these issues by constructing nanostructured sulfur cathodes, confining the sulfur within a conductive framework, such as nanoporous carbon,[8–12] graphene,[13,14] conductive polymer,[15–17] and metal oxides.[5,18–21] Although employing a matrix to constrain the sulfur could significantly improve the conductivity and alleviate the dissolution of polysulfides, there is still a significant amount of polysulfide dissolved into the electrolyte, especially under long cycling and high sulfur loading. Recently, various configurations of Li-S cell have been considered as an alternative approach to address the shuttle effect.[22–27] Many advanced interlayers fabricated from microporous carbon,[23] carbon nanotubes,[24] carbon nanofibers,[25] and graphene oxide [26] have been inserted between the cathode and separator in the cell configuration, which could greatly decrease the charge transfer resistance and trap the soluble polysulfides, resulting in improved utilization efficiency of the active materials and enhanced cyclability of the batteries. On the other hand, functionalizing the separator in Li-S batteries is also an effective route to preventing the diffusion of polysulfides across the separator. This can be achieved by introducing a coating layer on the cathode side of separator, such as with Nafion-coated, carbon-coated, and graphene-oxide-coated separators.[28–30] A complicated synthetic process and additional cost would be introduced in applying these strategies, however, so a much simpler and more cost effective construction would be more desirable for the large-scale fabrication and real applications.

Inspired by this need, we have designed an integrated flexible cathode architecture consisting of a carbon/sulfur/carbon sandwich structure spread directly on a polypropylene (PP) separator (CSC@separator) using the simple doctor-blading technique, in which commercial sulfur and Super P carbon (surface area of 64.56 $m^2 g^{-1}$; Supporting Information, Figure S1) are used as the raw materials to be coated on the PP separator as the sulfur layer and carbon layer, respectively.

An illustration of the cell configuration using a conventional electrode and the CSC@separator electrode is shown in Figure 1 a,b. Compared to the conventional electrode configuration, the CSC@separator electrode, where the CSC sandwich layers are directly coated on the separator without using aluminium (Al) foil as a substrate, greatly reduces the weight of the electrode (the weight of the substrate is reduced by 78%, 1.13 mg cm^{-2} for the separator and 5.30 mg cm^{-2} for Al foil) and exhibits excellent flexibility. The two carbon layers next to the sulfur layer could not only act as double current collectors from top to bottom to accelerate electron transport into the active material, but also serve as physical barriers to buffer the volume changes during cycling, preventing active material exfoliation and maintaining the integrity of the whole electrode. In addition, the double carbon coating layers work as an effective reservoir to trap the dissolved polysulfides within the cathode region, without affecting the lithium ion diffusion (Figure S2), resulting in

[*] H. Q. Wang, Prof. Z. P. Guo
Hubei Collaborative Innovation Centre for Advanced Organic Chemical Materials
Ministry of Education Key Laboratory for the Synthesis and Application of Organic Functional Molecules and
College of Chemistry and Chemical Engineering
Hubei University
Wuhan 430062 (P.R. China)
E-mail: zguo@uow.edu.au
H. Q. Wang, W. C. Zhang, Prof. H. K. Liu, Prof. Z. P. Guo
Institute for Superconducting & Electronic Materials
University of Wollongong
NSW 2500 (Australia)

Supporting information for this article can be found under http://dx.doi.org/10.1002/anie.201511673.

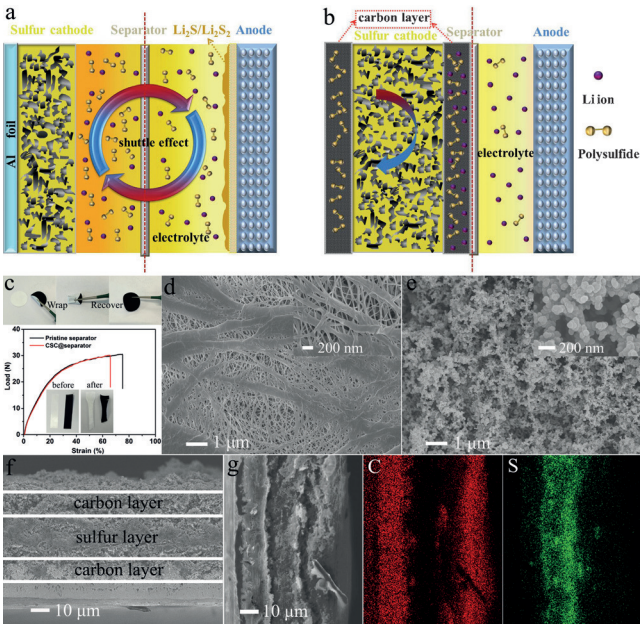

Figure 1. Illustration of Li-S cell configurations employing a) conventional electrode and b) integrated sandwich-structured electrode. c) Digital photographs and load-strain curves of the pristine separator and CSC@separator electrodes. SEM images of the surface of d) the pristine separator and e) the CSC@separator electrode. f) Cross-section of CSC@separator electrode and g) corresponding elemental mapping.

suppression of the shuttle effect and improved long-lasting cycling stability. Lastly, the utilization of commercial sulfur powders and Super P carbon as raw materials and the mature doctor-blade process make it an easy, low-cost, and scalable approach.

The as-prepared integrated CSC@separator electrode shows excellent flexibility, strong adhesion, and high mechanical strength (Figure 1 c). The bare separator displays a highly nanoporous structure with pore size around several hundred nanometers (Figure 1 d). In contrast, the CSC@separator electrode shows nanoparticle clusters on one side (Figure 1 e), while the other side of the electrode still keeps its nanoporous structure (Figure S3). The loose structure of the carbon coating layer ensures that the liquid electrolyte penetrates easily into the whole sandwich structure, and so that the electrochemical reactions proceed. The sandwich structure of the electrode can be further examined in the cross-sectional scanning electron microscope (SEM) image (Figure 1 f). The sandwich structure strongly adheres to the separator as an integrated electrode. The thicknesses of the carbon coating layers and the sulfur layer are about 10 μm and 20 μm, respectively. The elemental mapping results (Figure 1 g) clearly confirm the layered carbon/sulfur/carbon sandwich structure. The weight of two carbon layers is around 0.38–0.52 mg cm^{-2}, much lighter than the weight of the sulfur layer at 1.0–1.4 mg cm^{-2}. Even including the weight of the carbon coating layers, the content of sulfur in the whole electrode is still around 50 %.

To demonstrate the effectiveness of the integrated CSC@separator electrode, a series of electrodes were prepared for comparison, including a sulfur layer, a dual sulfur/carbon layer, and a dual carbon/sulfur layer coated on the separator (S@separator, SC@separator, and CS@separator, respectively), and the same sulfur content mixed with Super P and binder coated on Al foil (S@Al foil). The area of integrated electrode is the same as that of S@Al foil electrode. Surprisingly, all integrated separator electrodes showed enhanced utilization efficiency of sulfur and cycling stability at 0.2 C (1 C = 1000 mA g^{-1}), compared to the S@Al foil electrode (Figure 2 a). The CSC@separator electrode showed the highest reversible capacity and the best cycling stability, which is attributed to the integrated structure of the electrode and decreased charge transfer resistance (Figure 2 b). Furthermore, the CSC@separator electrode showed overlapping voltage plateaus and lower polarization compared to the S@Al foil electrode (Figure 2 c,d). The charge–discharge potential difference (ΔE) of the cells with CSC@separator electrode remained almost constant with cycle number, while the ΔE increases with cycling for the cell with S@Al foil

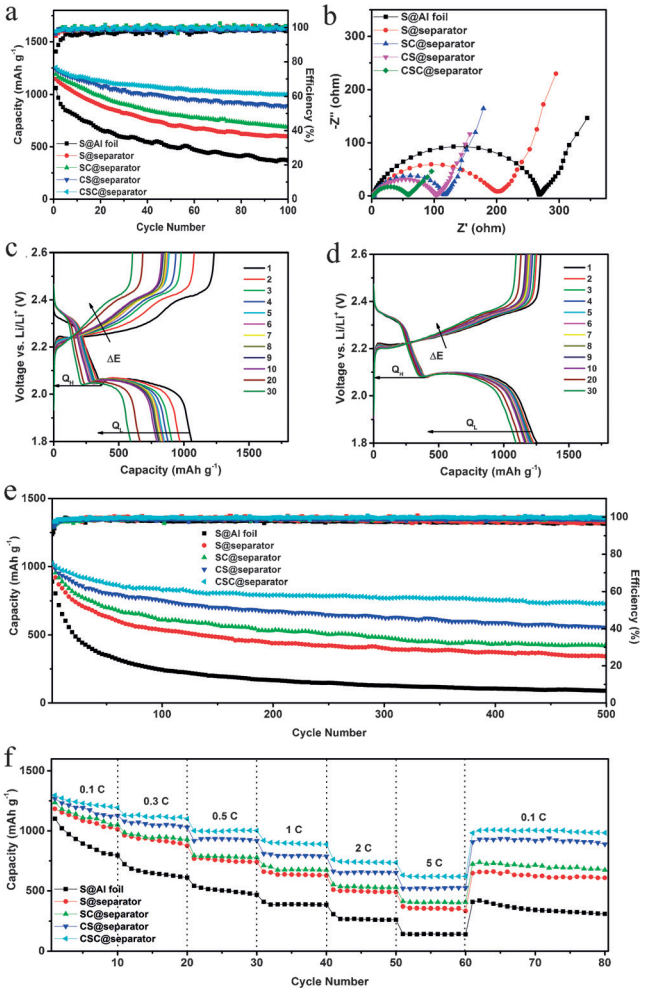

Figure 2. a) Cycling stability (0.2 C, 1 C = 1000 mA g^{-1})and b) electrochemical impedance spectroscopy of Li-S cells using S@Al foil and a series of integrated electrodes. Charge–discharge profiles for selected cycles of Li-S cells with c) S@Al foil and d) CSC@separator electrodes. e) Long-term cycling performance and f) rate capability of Li-S cells with S@Al foil, and a series of integrated electrodes at 0.6 C.

electrode (Figure S4). A similar tendency for ΔE was observed when the cells were tested at different current densities (Figure S5), indicating improved redox reaction kinetics and reversibility of the system. It was reported that the upper discharge plateau at 2.3 V represents the reduction reaction from sulfur to high-order soluble polysulfides.[29] Therefore, the high retention rate of discharge capacity (Q_H; Figure S6), corresponding to the upper plateau for the CSC@separator electrode, indicates that the carbon coating layers have strong polysulfide-trapping capability.

The long-term cycling stability of the CSC@separator electrode was studied at 0.6 C for 500 cycles (Figure 2 e), and the capacity stabilized around 730 mAh g^{-1}, corresponding to 71.2 % capacity retention and a small capacity fading of only 0.058 % per cycle. It should be noted that our integrated CSC@separator electrode prepared from commercial sulfur and Super P can still exhibit such a robust electrochemical performance. If nanostructured sulfur materials, such as sulfur–TiO_2 yolk shell nanoarchitecture,[19] can be used to fabricate the sulfur layer in our configuration design, a superior electrochemical performance could be obtained. Moreover, the highly reversible CSC@separator electrode delivered capacities of 1220, 1120, 1000, 900, 740, and 620 mAh g^{-1} at 0.1, 0.3, 0.5, 1, 2, and 5 C, respectively, confirming the excellent rate capability (Figure 2 f). It should be also pointed out that the introduction of the two carbon coating layers does not notably degrade the lithium ion conductivity, as confirmed by the similar diffusion coefficients of S@Al foil and the CSC@separator electrodes (Figure S2).

The integrated CSC@separator electrode also offers notable improvement of the self-discharge behavior in Li-S batteries. The severe self-discharge behavior mainly arises from the dissolution of sulfur during long-term storage, as can be clearly observed in the cells with S@Al foil electrode (Figure 3 a and Figure S7), causing a capacity loss of 37.8 % of its original capacity after 2 weeks storage. However, the cell with CSC@separator electrode showed almost identical discharge curves and low capacity loss of 14.5 % (Figure 3 b), indicating that the sulfur materials are well controlled within the double carbon layers, resulting in low self-discharge constant K_s of 0.0293 per week (Figure 3 c and Table S1). The static electrochemical stability of the S@Al foil electrode and the CSC@separator electrodes is shown in Figure 3 d,e. After resting for 4 weeks, the cell with the CSC@separator electrode still showed good cycling stability, with a high initial capacity retention of 81.3 %. After 20 cycles, the CSC@separator electrode delivered much higher reversible capacity after resting for 3 weeks. The significantly improved static capacity retention indicates that the double carbon coating layer in the sandwich structure serves as a protective layer, preventing the sulfur material from dissolving into the electrolyte, and thus eliminating the severe self-discharge problem that occurs in the conventional Li-S cells.

Figure 4 a presents digital photographs of the S@Al foil and CSC@separator electrodes after 100 cycles. A small amount of active materials exfoliated from the S@Al foil electrode. In contrast, the CSC@separator electrode maintained a good appearance, without any obvious exfoliation or changes, indicating good structural stability. Furthermore, the

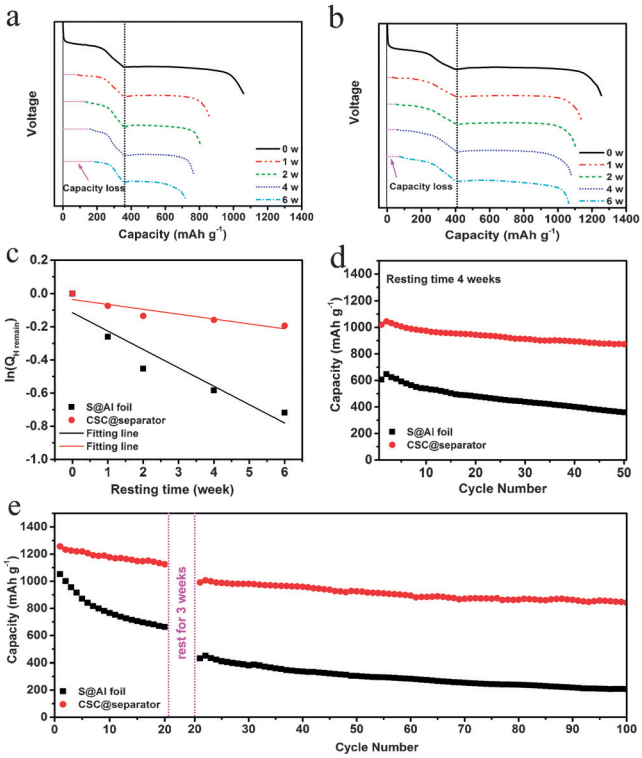

Figure 3. a) Initial discharge profiles of Li-S cells with S@Al foil and b) CSC@separator electrodes after different open-circuit durations at current density of 0.2 C. c) Natural logarithm of the retention rate of upper plateau discharge capacity as a function of resting time for calculating the self-discharge constant. d) Cycling performances of the cells containing S@Al foil and CSC@separator electrodes after 4 weeks storage and e) with 3 weeks resting time after 20 cycles at 0.2 C.

cycled S@Al foil and CSC@separator electrodes were examined by ultraviolet/visible (UV/Vis) absorption spectroscopy. The color of the DOL/DME solutions for the S@Al foil electrodes changed from colorless to yellow with increasing cycle number, while no noticeable color change was observed for the CSC@separator electrodes (Figure S8). The similar intensities of the peaks for the CSC@separator electrodes at different cycles indicate similar content of polysulfides in the electrolyte, confirming a low rate of polysulfide diffusion and effective absorption by the double carbon layers (Figure 4 b). The morphology of the cycled S@Al foil and CSC@separator electrode was studied by SEM (Figure S9). After 100 cycles, the surface of the S@Al foil electrode became denser, and large particle aggregation was clearly observed. The elemental mapping and energy-dispersive X-ray (EDX) spectroscopy results revealed that the particle aggregates are rich in sulfur. In contrast, the CSC@separator electrode showed no obvious changes, and no particle aggregation and a weak signal of sulfur, suggesting that the diffusion of polysulfide is controlled within the two carbon layers. To further confirm the effects of the carbon layer in suppressing the diffusion of the polysulfides, a cross-sectional SEM image and a schematic illustration of polysulfide diffusion in the CSC@separator electrode are shown in Figure 4 c–e. The sandwich structure of the CSC@separator electrode was still maintained after

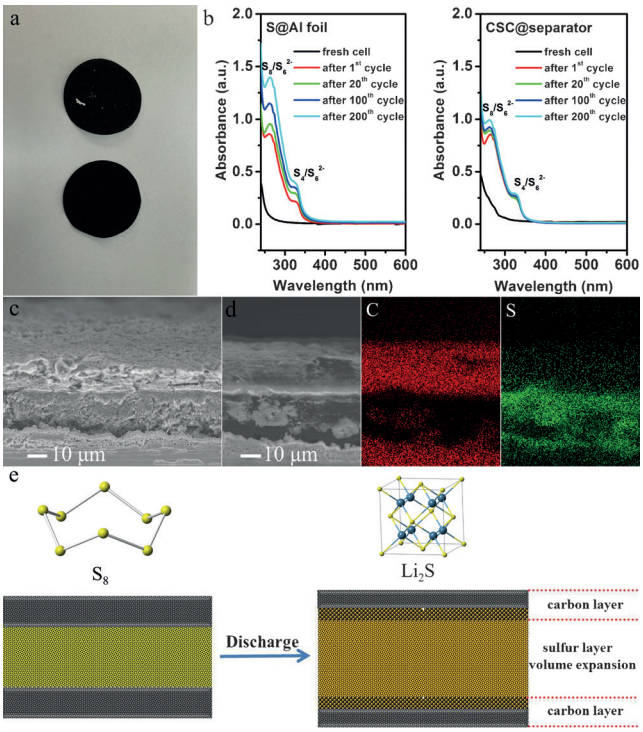

Figure 4. a) Digital photographs of S@Al foil (top) and CSC@separator electrodes (bottom) after 100 cycles. b) UV/Vis absorption spectra of DOL/DME solution with S@Al foil electrode and CSC@separator electrode at various cycle numbers. c) SEM image and d) elemental mapping of the cross-section of CSC@separator after 100 cycles. e) Illustration of polysulfide diffusion, with trapping between the carbon layers.

100 cycles, demonstrating the excellent structural stability of the integrated electrode, which could control the diffusion of polysulfides, buffer the volume changes during cycling, and maintain the integrity of the whole electrode.

To further understand why the integrated electrode could delivery more stable capacity than the conventional S@Al foil electrode, the cycling performance of a half-covered S@separator electrode was tested (Figure S10). There was a small amount of Super P in the S@separator electrode, which could easily disperse into the nanopores of the separator and act as a complete physical barrier to prevent polysulfide diffusion to the anode side for a fully covered S@separator electrode. However, the uncovered surface in the half-covered S@separator electrode resulted in poor cycling performance. Commonly, no matter how sophisticated the nanostructured sulfur cathode is in a conventional Li-S cell, it is inevitable that small amounts of polysulfides will dissolve into the electrolyte and then diffuse across the nanoporous separator, leading to the capacity fading. In our design, however, the dissolved polysulfides must travel through the carbon coating layer before the separator, fully encountering the absorption effect of the carbon layer. The carbon layers could serve as effective barriers to control the diffusion of the polysulfides and keep them within the cathode region, eliminating the shuttle effect and self-discharge behavior. The shuttle factor for the CSC@separator electrode is 0.067, much lower than that for the S@Al foil electrode (0.42, Table S2).

In summary, we have successfully designed and prepared a unique flexible cathode architecture consisting of a carbon/sulfur/carbon sandwich structure coated directly on a PP separator using the doctor-blade method. The CSC@separator cathode delivered a high reversible capacity of 730 mAh g^{-1} over 500 cycles, with capacity decay as small as 0.058% per cycle and a low self-discharge constant of 0.0293 per week. This improved performance is attributed to the enhanced electronic conductivity, toleration of volume expansion, and control of the polysulfide diffusion by the integrated sandwich-structured electrode. Together with the simple and scalable nature of its fabrication, our electrode is highly promising for practical applications in Li-S batteries.

Acknowledgements

Financial support provided by the Australian Research Council (ARC) through an ARC Discovery project (DP1094261) is gratefully acknowledged. Moreover, the authors would like to thank Dr. Tania Silver for critical reading of the manuscript and valuable remarks.

Keywords: integrated flexible cathodes · lithium–sulfur batteries · self-discharge · shuttle effect

How to cite: *Angew. Chem. Int. Ed.* **2016**, *55*, 3992–3996
Angew. Chem. **2016**, *128*, 4060–4064

[1] S. E. Cheon, S. S. Choi, J. S. Han, Y. S. Choi, B. H. Jung, H. S. Lim, *J. Electrochem. Soc.* **2004**, *151*, A2067–A2073.
[2] X. L. Ji, K. T. Lee, L. F. Nazar, *Nat. Mater.* **2009**, *8*, 500–506.
[3] P. G. Bruce, S. A. Freunberger, L. J. Hardwick, J. M. Tarascon, *Nat. Mater.* **2012**, *11*, 19–29.
[4] Y. Yang, G. Y. Zheng, S. Misra, J. Nelson, M. F. Toney, Y. Cui, *J. Am. Chem. Soc.* **2012**, *134*, 15387–15394.
[5] Z. Li, J. T. Zhang, X. W. Lou, *Angew. Chem. Int. Ed.* **2015**, *54*, 12886–12890; *Angew. Chem.* **2015**, *127*, 13078–13082.
[6] N. Jayaprakash, J. Shen, S. S. Moganty, A. Corona, L. A. Archer, *Angew. Chem. Int. Ed.* **2011**, *50*, 5904–5908; *Angew. Chem.* **2011**, *123*, 6026–6030.
[7] H. L. Wang, Y. Yang, Y. Y. Liang, J. T. Robinson, Y. G. Li, A. Jackson, Y. Cui, H. J. Dai, *Nano. Lett.* **2011**, *11*, 2644–2647.
[8] C. Zhang, H. B. Wu, C. Yuan, Z. Guo, X. W. Lou, *Angew. Chem. Int. Ed.* **2012**, *51*, 9592–9595; *Angew. Chem.* **2012**, *124*, 9730–9733.
[9] Q. Pang, J. T. Tang, H. Huang, X. Liang, C. Hart, K. C. Tam, L. F. Nazar, *Adv. Mater.* **2015**, *27*, 6021–6028.
[10] L. N. Wang, Y. Zhao, M. L. Thomas, H. R. Byon, *Adv. Funct. Mater.* **2014**, *24*, 2248–2252.
[11] J. X. Song, M. L. Gordin, T. Xu, S. R. Chen, Z. X. Yu, H. Sohn, J. Lu, Y. Ren, Y. H. Duan, D. H. Wang, *Angew. Chem. Int. Ed.* **2015**, *54*, 4325–4329; *Angew. Chem.* **2015**, *127*, 4399–4403.
[12] Q. Sun, X. Fang, W. Weng, J. Deng, P. N. Chen, J. Ren, G. Z. Guan, M. Wang, H. S. Peng, *Angew. Chem. Int. Ed.* **2015**, *54*, 10539–10544; *Angew. Chem.* **2015**, *127*, 10685–10690.
[13] M. Q. Zhao, Q. Zhang, J. Q. Huang, G. L. Tian, J. Q. Nie, H. J. Peng, F. Wei, *Nat. Commun.* **2014**, *5*, 3410.
[14] J. P. Rong, M. Y. Ge, X. Fang, C. W. Zhou, *Nano Lett.* **2014**, *14*, 473–479.
[15] J. L. Wang, Y. S. He, J. Yang, *Adv. Mater.* **2015**, *27*, 569–575.

[16] L. F. Xiao, Y. L. Cao, J. Xiao, B. Schwenzer, M. H. Engelhard, L. V. Saraf, Z. M. Nie, G. J. Exarhos, J. Liu, *Adv. Mater.* **2012**, *24*, 1176 – 1181.
[17] K. Park, J. H. Cho, J. H. Jang, B. C. Yu, A. T. De La Hoz, K. M. Miller, C. J. Ellison, J. B. Goodenough, *Energy Environ. Sci.* **2015**, *8*, 2389 – 2395.
[18] X. Liang, A. Garsuch, L. F. Nazar, *Angew. Chem. Int. Ed.* **2015**, *54*, 3907 – 3911; *Angew. Chem.* **2015**, *127*, 3979 – 3983.
[19] Z. W. Seh, W. Y. Li, J. J. Cha, G. Y. Zheng, Y. Yang, M. T. McDowell, P. C. Hsu, Y. Cui, *Nat. Commun.* **2013**, *4*, 1331.
[20] Q. Pang, D. Kundu, M. Cuisinier, L. F. Nazar, *Nat. Commun.* **2014**, *5*, 4759.
[21] Z. Liang, G. Y. Zheng, W. Y. Li, Z. W. Seh, H. B. Yao, K. Yan, D. S. Kong, Y. Cui, *ACS Nano* **2014**, *8*, 5249 – 5256.
[22] K. E. Hendrickson, L. Ma, G. Cohn, Y. Y. Lu, L. A. Archer, *Adv. Sci.* **2015**, *2*, 1500068.
[23] Y. S. Su, A. Manthiram, *Nat. Commun.* **2012**, *3*, 1166.
[24] Y. S. Su, A. Manthiram, *Chem. Commun.* **2012**, *48*, 8817 – 8819.
[25] J. Q. Huang, B. A. Zhang, Z. L. Xu, S. Abouali, M. A. Garakani, J. Q. Huang, J. K. Kim, *J. Power Sources* **2015**, *285*, 43 – 50.
[26] X. F. Wang, Z. X. Wang, L. Q. Chen, *J. Power Sources* **2013**, *242*, 65 – 69.
[27] S. H. Chung, A. Manthiram, *Chem. Commun.* **2014**, *50*, 4184 – 4187.
[28] J. Q. Huang, Q. Zhang, H. J. Peng, X. Y. Liu, W. Z. Qian, F. Wei, *Energy Environ. Sci.* **2014**, *7*, 347 – 353.
[29] S. H. Chung, A. Manthiram, *Adv. Mater.* **2014**, *26*, 7352 – 7357.
[30] J. Q. Huang, T. Z. Zhuang, Q. Zhang, H. J. Peng, C. M. Chen, F. Wei, *ACS Nano* **2015**, *9*, 3002 – 3011.

Received: December 16, 2015
Revised: January 25, 2016
Published online: February 17, 2016

